

Distinctive VEGFR2 Endocytic Delivery during Muscle Mobilization

Han-Wei Huang and Hui Zhao*

Department of Integrative Medicine and Neurobiology, National Key Lab of Medical Neurobiology, Institute of Brain Sciences, Fudan University, Shanghai, China

*Corresponding author: Hui Zhao, Department of Integrative Medicine and Neurobiology, National Key Lab of Medical Neurobiology, Institute of Brain Sciences, Fudan University, Shanghai, China, Tel: 86-21-54237611; E-mail: zhaohui07054@fudan.edu.cn

Received date: March 11, 2015; Accepted date: June 02, 2015; Published date: June 08, 2015

Copyright: © 2015 Huang H, et al. This is an open-access article distributed under the terms of the Creative Commons Attribution License, which permits unrestricted use, distribution, and reproduction in any medium, provided the original author and source are credited.

Abstract

Denervation of skeletal muscles initiates a cascade of cellular events that can lead to muscle atrophy, however, the underlying mechanism is controversial. In the present study, by using techniques including real-time PCR, immunoblotting, fluorescent in situ hybridization, and enzyme-linked immunosorbent, we demonstrated that VEGFR2 was distinctively cross-linked with MyHC1 in gastrocnemius, and MyHC2B in soleus, which was likely responsible for activation of receptor tyrosine kinases including growth factor receptor-bound 2, phospholipase Cy, p85, Vav, and human epidermal growth factor receptor 2. When challenged with muscle mobilization, in gastrocnemius, VEGFR2 was preferentially translocated into mitochondria, which resulted in activation of NAD⁺-SIRT1 and remodel of macrophage polarization. Alternatively, in soleus, VEGFR2 was targeted to ER, this short-range transport eventually enhanced T cell activation including miR181a expression and IL-15 release. Importantly, M1 macrophage polarization and T cell activation mostly induced disrupted muscular homeostasis, the cellular processes might make soleus more vulnerable to insults than gastrocnemius. Therefore, endocytic delivery of VEGFR2 by myosin might precipitate distinctive cellular environment in the mobilized gastrocnemius and soleus, mitochondrial gene transcription and T cell activation were proposed to involve in the phenotype-dependent alterations respectively.

Keywords: Muscle mobilization; Myosin; VEGFR-2; Macrophage polarization; T cell activation

Abbreviations:

VEGFR2: Vascular Endothelial Growth Factor Receptor 2; MyHC: Myosin Heavy Chain; NAD⁺: Nicotinamide Adenine Dinucleotide; SIRT1: Sirtuin 1; PGC-1α: α-Subunit of Peroxisome Proliferators-activated Receptor-γ Coactivator-1; ER: Endoplasmic Reticulum; ELISA: Enzyme-Linked Immunoassay; NOS: Inducible Nitric Oxide Synthase; IL-1β: Interleukin-1β; IFN-γ: Interferon-γ; Trem 2: Triggering Receptor Expressed on Myeloid Cells 2; MuSK: Muscle-Specific Kinase; AchR: Acetylcholine Receptor

Introduction

Skeletal muscle comprises up to 40% of human body mass, and is a highly ordered, structurally stable tissue whose function is dependent on an intact nerve supply. Sciatic nerve injury causes profound structural and functional changes to target muscles, including rapid loss of muscle mass and contractile force [1,2]. As reported, mitochondrial biogenesis is associated with PGC-1α, playing a critical role in metabolic and inflammatory responses by regulating NAD⁺ production [3-5] and deacetylase SIRT1 [6-9], the induced changes are implicated in glycolysis and chromatin compaction of proinflammatory genes. Our previous observation indicated that vascular endothelial growth factor (VEGF)-VEGF receptor (R)2 signaling was initiated during muscle denervation, which was under the control of muscular inflammation and mitochondrial biogenesis, and accompanied with ensuing changes in the motor endplate [10-12]. Since macrophage polarization occurs during the course of wound healing [13-18], and is defined by classical (M1) and alternative (M2) activation states that mediate pathogen destruction and tissue

remodelling [19-23], thereby, whether VEGFR2 signaling can promote macrophage polarization during muscle mobilization is yet to be determined.

Skeletal muscles differ with respect to the size of the constituent motor units, fiber types could be distinguished based on the presence of MyHC-1/slow and MyHC-2B/fast isoforms [24]. Also, motor endplates on fast and slow muscle fibers show distinct transmitter release characteristics [25]. Accumulating evidence indicated that the degree of muscle denervation depends on muscle type, with atrophy more prominent in type I than in type II muscle fibers [26-29]. There is also a differential turnover of MyHC proteins during muscle wasting after a bed-rest period, which is indicative of muscle fibers in a transitional state [30]. Recently, it was reported that VEGFR2 turnover at the plasma membrane is mediated through a myosin-dependent mechanism, which reinforces cellular processes such as endosomal recycling or vesicle trafficking [31]. As such, the present study is designed to investigate the association of short-range VEGFR2 cargo by myosin and functional muscular stabilization during muscle mobilization. A better understanding of phenotype-dependent alterations in muscle would enable the development of new agents to combat degenerative muscular disorders.

Materials and Methods

Muscle mobilization and ethics statement

Male SD rats (160-180 g, n=6 for each group) were anesthetized with isoflurane (inhalation, 4%, at a flow of 2 L/h and take around 9.5 ± 1.7 ml for each rat), and the lower right leg was casted from the knee to the toes with heat-activated casting material (Vet Lite, Kruuse, Marslev, Denmark). After casting, animals were euthanized by carbon dioxide asphyxiation (90.1 ± 4.3% for each rat). Then the cast was

removed, gastrocnemius and soleus muscles (1×1 cm, 50 mg) were dissected rapidly from both legs, and were cleaned of tendons and connective tissue and weighed. All experimental protocols were approved by Ethics Committee of Fudan University, and in accordance with the relevant codes of practice for the care and use of animals for scientific purposes (National Institutes of Health, 1985). All efforts were made to minimize the numbers of animal used and their suffering.

Recombinant adenovirus construction

Recombinant adenovirus were constructed by inserting rat VEGFR2, mitoVEGFR2, or SirT1 siRNA into adenoviral shuttle vector pDE1sp1A (Microbix Biosystems, Inc. Canada), the insert was then switched to the adenoviral vector through LR recombination. After homologous recombination with the backbone vector PJM17, plaques resulting from viral cytopathic effects were selected and expanded in 293 cells, positive plaques were further purified and large-scale production of adenovirus was carried out by two sequential CsCl gradients and PD-10 Sephadex chromatography.

Mitochondrial DNA assay

Total DNA was extracted from 10 µg of muscles using the QIAampDNA Mini Kit (Qiagen, Germany), and quantitative PCR was performed using mitochondrial DNA and genomic DNA-specific primers. The 18S rRNA gene served as the endogenous reference gene. Melting curves were obtained to ensure specific amplification, and the standard curve was used for relative quantification. Final results are expressed as n-fold differences in mitochondrial D-loop expression relative to that of 18S rRNA gene.

Nerve-muscle preparations

Soleus and gastrocnemius muscles, with their respective motor nerve, were dissected from rats under deep anesthesia. Nerve-muscle preparations were pinned in Sylgard-coated recording chamber filled with normal Ringer's solution containing (in mM): 124 NaCl, 5 KCl, 1.25 NaH₂PO₄, 2 MgCl₂, 1NaHCO₃, 2 CaCl₂, 25 HEPES and 10 glucose, oxygenated with 100% O₂. A 2-3 mm broad band of muscle around innervated muscle was excised, representing the junctional region. For M1 macrophage induction, lipopolysaccharide (LPS, 100 ng/mL) and interferon-gamma (IFNγ, 20 ng/mL) were added to macrophage cultures for 48 hours; For macrophage M2 induction, interleukin 4 (IL-4; 20 ng/mL) was added to the cultures for 48 hours; Conditioned medium was collected and concentrated using Amicon ultra centrifuge filters (Millipore, Billerica, MA, USA). Nerve-muscle preparation was exposed to conditioned medium or IL-15 (20 ng/mL) for 48 hours respectively.

ELISA assay

Levels of M1 macrophage (iNOS, IL-1β, IL-6, IFNγ), M2 macrophage (Arg1, Ym1, Trem2, IL-4) and IL-15 production were measured by ELISA according to the manufacturer's instructions (R&D Systems, Inc., Minneapolis, MN). A 96-well plate was coated with 2 µg/ml monoclonal antibodies at 4°C overnight and then blocked with 1% bovine serum albumin (BSA) in PBS for 1 h. 100 µl of tissue lysates diluted with Hanks' balanced salt solution (HBSS) were added to the plates, and incubated for 2 h at room temperature. After washes three times with PBS, 100 µl of 0.1 µg/ml biotinylated polyclonal antibodies were added and incubated for 2 h. After further

washes with PBST, the immune complexes were colorimetrically detected using horseradish peroxidase (HRP)-streptavidin conjugate. The reaction was halted by addition of 1 M H₂SO₄, the absorbance at 450 nm was measured using a microplate reader (VERSAmax; Molecular Devices, Sunnyvale, CA).

Evaluation of NAD⁺/NADH Ratio

Total cellular NADt (NAD⁺/NADH) evaluation were performed using a colorimetric NAD⁺/NADH assay kit (BioVision) according to manufacturer's instructions. NADt extractions were filtered by passing samples through a 10 Kd molecular weight cutoff filter to exclude the possible NADH consuming enzymes. The optical density was read at 450 nm. NADt levels were calculated from the standard curve and normalized against protein levels. NAD⁺ levels were obtained by subtraction of the NADH level from NADt, the ratio of NAD⁺/NADH was calculated as (NADt-NADH)/NADH.

Lipid raft fraction separation

Muscles were washed twice with phosphate-buffered saline (pH 7.4) at 4°C and dissolved into 2 ml of 500 mM sodium carbonate (pH 11.0) solution with 400µl protease inhibitor cocktail (Roche Applied Science) followed by 10 strokes of homogenization, and sonication with one 30-s burst at setting 4 and one 30-s burst at setting 7 (model W-220F, Ultrasonics, Inc.). The homogenate was adjusted to 45% sucrose by adding 2 ml of 90% sucrose prepared in MBS buffer (25 mM MES, pH 6.5, and 0.15 M NaCl) and placed at the bottom of an ultracentrifuge tube. Then 4 ml of 35% sucrose and 4 ml of 5% sucrose (both in MBS buffer containing 250 mM sodium carbonate) were loaded to form a 5-45% discontinuous sucrose gradient. The sample was centrifuged at 160,000g for 16 h in a Beckman L7 ultracentrifuge with an SW-41Ti rotor. Fractions of 1 ml each were collected from the top, in which fractions 4 and 5 were considered to be lipid raft-rich fractions.

Immunoprecipitation and Western Blotting

Muscles were homogenized and incubated with anti-MyHCl, antiMyHC2B or AchRa antibody (1:200; BD Transduction Laboratories, Lexington, KY) at 4°C overnight with slow rotation. 60 µl of protein G-agarose beads (Invitrogen, Carlsbad, CA) were added and further incubated for 3 h. Afterwards, the beads were washed and protein sample were eluted with 1x SDS sample buffer. For Western blot analysis, protein samples were resolved by sodium dodecylsulfate polyacrylamide gel electrophoresis (SDS-PAGE) and transferred to polyvinylidene difluoride membranes (GE Healthcare, Piscataway, NJ). Membranes were probed with anti-VEGFR2 (1:1000; Abcam, Cambridge, MA), anti-AchRβ (1:500; Abcam), anti-Grb2/PLCγ/P85/Vav/HER2 (1:1000; BD Transduction Laboratories, Lexington, KY), anti-SirT1 antibodies (1:500, Abcam), respectively. Protein bands were detected using alkaline phosphatase conjugated secondary antibody (1:5000) and ECF substrate, and scanned with Storm 860 imaging system. Band intensities were quantified and analyzed with ImageQuant software (GE Healthcare).

miR181a fluorescent in situ hybridization (FISH)

SD rats were anesthetized with sodium pentobarbital (35 mg/100 g, i.p.) and transcardially exsanguinated with 0.1M PBS followed by perfusion of the fixation (4% paraformaldehyde in 0.1M PBS, pH 7.4) at a 7ml/min flow rate, serial sets of 10 µm coronal sections were

collected on a freezing microstome (Leica, SM2000R). Hybridization was performed with a locked nucleic acid (LNA)-modified, 5'-digoxigenin-labeled probe of miR-181a (Exiqon) at a concentration of 40 nM. Following hybridization, a stringency wash was performed with a descending gradient of saline-sodium citrate ($5\times$, $2\times$ and $0.2\times$) at 4°C, then probes were detected using Alexa Fluor488-conjugated anti-DIG antibody. Data derived from each group were analyzed by Leika Q500IW image analysis system, hybridization density is reported as the average density of individual animal \pm SEM in each experimental group (n=6). The mean density of all the microphotographs was analyzed with the aid of ImageJ analysis software.

In vitro Src or MuSK kinase assay

Proteins in anti-VEGFR-2 or anti-MuSK antibody immunoprecipitated pool (1:200; Abcam) were precipitated with 5% (w/v) TCA. The resulting pellets were washed with acetone and incubated at 30°C with 5 µg of SRC substrate peptide (KVEKIGEGTYGVVYK, corresponding to amino acids 6-20 of p34cdc2; Upstate Biotechnology, Lake Placid, New York) in kinase buffer containing 5 µCi of [γ -³²P]-adenosine triphosphate ([γ -³²P]-ATP; PerkinElmer Life Sciences, Waltham, Massachusetts), 50 mM Tris-HCl (pH 7.5), 10mM MgCl₂, 10 mM MnCl₂, 25 µM ATPase, 1 mM dithiothreitol, and 100 µM Na₃VO₄. After 30 min, the reaction was terminated by 10 µl of 40% (w/v) TCA, and samples were spotted on P81 cellulose phosphate paper (Upstate Biotech). Radioactivity retained on the P81 paper was quantified by liquid scintillation counting. Blank counts (without tissue lysate) were subtracted from each result, and radioactivity (cpm) was converted to picomoles per minute (pmol/min).

Whole muscle mechanical properties

The experiments were performed at 30°C in a vertical muscle apparatus (300B, Aurora Scientific) containing Ringer solution (120 mM NaCl, 4.7 mM KCl, 2.5 mM CaCl₂, 3.15 mM MgCl₂, 1.3 mM NaH₂PO₄, 25 mM NaHCO₃, 11 mM glucose, 30 µM d-tubocurarine, pH 7.2-7.4). The muscles were stretched to the optimal length that allowed maximal tension development in response to a single pulse. The muscles were then electrically stimulated through two parallel electrodes, with supramaximal pulses (0.5-ms duration) delivered by Grass S44 electronic stimulator, muscle response was recorded by isometric force transducer (Grass FT03). Tetanic stimulation was obtained by applying trains of supramaximal stimuli at 80- and 150-Hz frequency for the muscles, tetanic tension was normalized to the muscle wet weight (specific tension, N/g).

Statistics

Data were represented as mean \pm SEM and analyzed with Prism 5 software. For all data sets, normality and homocedasticity assumptions were reached, validating the application of the one-way ANOVA, followed by Dunnett test as post hoc test to do comparisons. Differences were considered significant for p<0.05.

Results

VEGFR2 is differentially recruited by myosin in slow and fast muscles during mobilization

It was previously reported that VEGFR2 could be initiated during muscle denervation [5]. In the present observation, immunoprecipitation experiments showed that the interaction between MyHCl and VEGFR2 was biphasically modulated during muscle mobilization, namely, increased within 7 days and then gradually decreased, the alteration occurred on gastrocnemius but not soleus (Figure 1A and 1B). Likewise, in gastrocnemius, Western Blot analysis indicated that expressions of receptor tyrosine kinase-related molecules including growth factor receptor-bound (Grb)2, phospholipase (PL) C γ , P85, Vav, and human epidermal growth factor receptor (HER)2 were markedly increased on days 1-7 following muscle mobilization, with levels that were 2.1-3.0 fold higher than control values (Figure 1C and 1D). However, above molecules were gradually down-regulated in the mobilized soleus (Figure 1E and 1F).

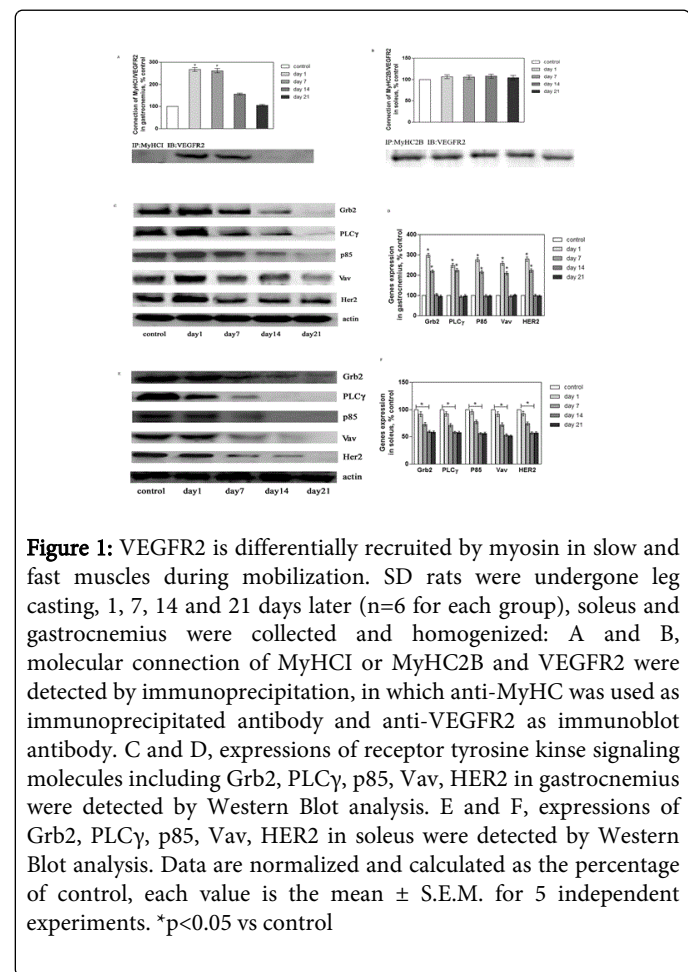


Figure 1: VEGFR2 is differentially recruited by myosin in slow and fast muscles during mobilization. SD rats were undergone leg casting, 1, 7, 14 and 21 days later (n=6 for each group), soleus and gastrocnemius were collected and homogenized: A and B, molecular connection of MyHCl or MyHC2B and VEGFR2 were detected by immunoprecipitation, in which anti-MyHC was used as immunoprecipitated antibody and anti-VEGFR2 as immunoblot antibody. C and D, expressions of receptor tyrosine kinase signaling molecules including Grb2, PLC γ , p85, Vav, HER2 in gastrocnemius were detected by Western Blot analysis. E and F, expressions of Grb2, PLC γ , p85, Vav, HER2 in soleus were detected by Western Blot analysis. Data are normalized and calculated as the percentage of control, each value is the mean \pm S.E.M. for 5 independent experiments. *p<0.05 vs control

In gastrocnemius, VEGFR2 is transported to mitochondria during muscle mobilization

By Western Blot analysis, it was illustrated that VEGFR2 expression in mitochondria fraction was increased by ~2.5-fold over the control value on days 14-21 after muscle mobilization, the alteration was restricted within gastrocnemius but not soleus (Figure 2A). In parallel,

mitochondrial DNA (mtDNA) content was increased in the mobilized gastrocnemius (Figure 2B). Meanwhile, Src kinase activity within mitochondria was quantified by the kinase-catalyzed phosphorylation of a synthetic Src-specific target peptide (corresponding to p34cdc2 amino acids 6-20) via incorporation of [γ -³²P]-ATP. As revealed in Figure 2C, an increase in mitochondria-associated Src kinase activity was observed only in gastrocnemius but not soleus, with radiolabel incorporation around 2.6-fold over control following 14-21 days of muscle mobilization. Moreover, in a nerve-muscle preparation, transfection of a mitochondria-targeted VEGFR2 (mitoVEGFR2) resulted in an elevation in mtDNA content and mitochondrial Src kinase activity (Figure 2D and 2E).

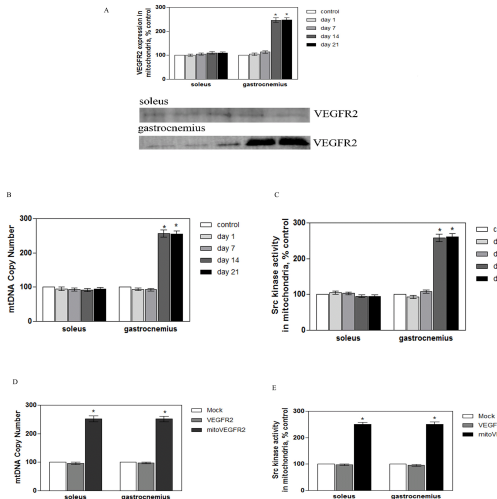


Figure 2: In gastrocnemius, VEGFR2 is transported to mitochondria during muscle mobilization. Rats were undergone leg casting, 1, 7, 14 and 21 days later (n=6 for each group), soleus and gastrocnemius were collected and homogenized. A, mitochondria was separated and VEGFR2 expression was carried out by Western Blot analysis; B, mitochondrial D-loop expression relative to that of the 18S rRNA gene was measured by real-time PCR; C, Src kinase activity was determined by *in vitro* kinase assay. Nerve-muscles were cultured in the presence of VEGFR2 or mitoVEGFR2 (affinity to mitochondria). D, mitochondrial D-loop expression relative to that of the 18S rRNA gene was measured by real-time PCR; E, Src kinase activity was determined by *in vitro* kinase assay. Data are normalized and calculated as the percentage of control, each value is the mean \pm S.E.M. for 5 independent experiments. *p<0.05 vs control or Mock.

soleus muscle, an effect that was enhanced by mitoVEGFR2 infection (Figure 3A). The concomitant upregulation of SIRT1 expression was also potentiated by mitoVEGFR2 infection (Figure 3B and 3C).

Moreover, when detected by ELISA, it was revealed that the expression of M1 markers (NOS, IL-1 β , IL-6, and IFN- γ) increased rapidly around 1.6-fold over control values in the mobilized gastrocnemius and soleus on days 1-7, while M2 markers (arginase 1, Ym1, Trem 2, and IL-4) were expressed in the same pattern in gastrocnemius but not soleus (Figure 3D and 3E). Notably, in nerve-muscle preparations, the expression of M1 and M2 macrophages could be enhanced and inhibited by NAD $^{+}$ -SIRT1 signaling respectively. The similar modulation was observed in the presence of VEGFR2 mitochondrial expression (Figure 3F and 3G).

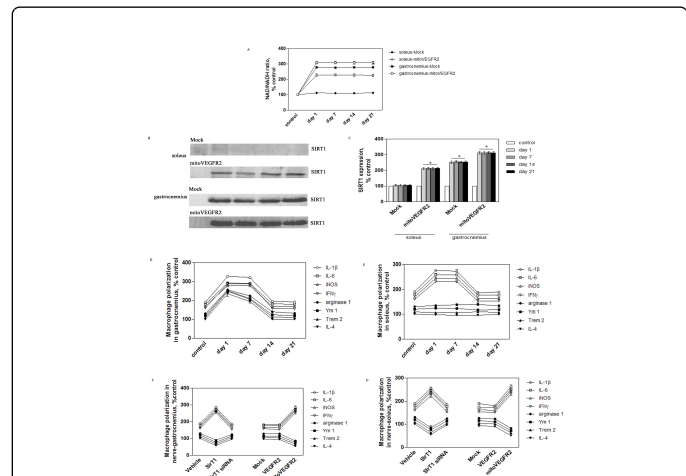


Figure 3: Nicotinamide adenine dinucleotide (NAD) $^{+}$ -sirtuin (SIRT1) expression and resultant macrophages phenotypes during muscle mobilization. Rats were locally infected with adeno-virus VEGFR2 or mitoVEGFR2, then undergone leg casting, 1, 7, 14 and 21 days later (n=6 for each group), soleus and gastrocnemius were collected and homogenized. A, NAD $^{+}$ level was measured by photometry; B and C, SIRT1 expression was detected by Western Blot analysis. Rats were undergone leg casting, 1, 7, 14 and 21 days later (n=6 for each group), soleus and gastrocnemius were collected and homogenized. D and E, macrophage markers for M1 (iNOS, IL-1 β , IL-6, IFN- γ) and M2 (arginase 1, Ym1, Trem2, IL-4) were detected by ELISA assay. F and G, Nerve-muscles were cultured and infected with adeno-SirT1 or SirT1 siRNA, adeno-virus VEGFR2 or mitoVEGFR2, macrophage markers for M1 and M2 were detected by ELISA assay. Data are normalized and calculated as the percentage of control, each value is the mean \pm S.E.M. for 5 independent experiments. *p<0.05 vs control.

In soleus, VEGFR2 is targeted to ER during muscle mobilization

By Western Blot analysis, expression level of VEGFR2 in ER fraction was upregulated by ~3.0-fold over the control following muscle mobilization, the alteration was restricted in soleus muscle (Figure 4A and 4B). Furthermore, immunoprecipitation experiments revealed that, the interaction between MyHC2B and VEGFR2 increased upon muscle mobilization (Figure 4C and 4D).

Coincidentally, it was demonstrated that in soleus but not gastrocnemius, translocation of calreticulin into lipid rafts was evoked following muscle mobilization, signal quantification revealed that the expression levels were elevated around 1.8 folds over control values (Figure 4E and 4F).

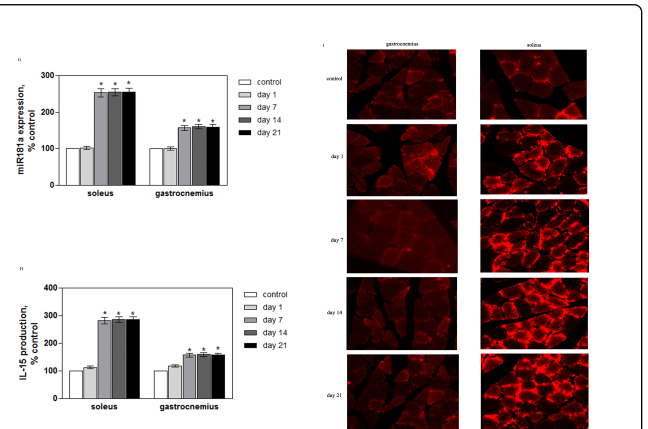
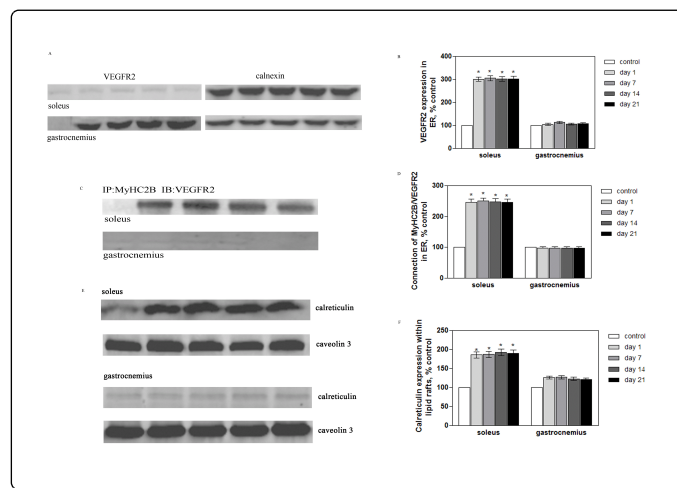


Figure 4: In soleus, VEGFR2 is targeted to endoplasmic reticulum (ER) during muscle mobilization. SD rats were undergone leg casting, 1, 7, 14 and 21 days later (n=6 for each group), soleus and gastrocnemius were collected and ER compartment was separated. A and B, VEGFR2 expression was detected by Western Blot analysis; C and D, molecular connection of MyHC2B and VEGFR2 were detected by immunoprecipitation, in which anti-MyHC2B was used as immunoprecipitated antibody and anti-VEGFR2 as immunoblot antibody; E and F, caveolin-3 enriched fraction was isolated, and expression of calreticulin was detected by Western Blot analysis; G and I, miR181a expression level was measured by real-time PCR and FISH assay, Scale bar=50 μm; H, production of IL-15 was measured by ELISA assay. Data are normalized and calculated as the percentage of control, each value is the mean ± S.E.M. for 5 independent experiments.

Together with above observation, by real-time PCR and Western Blot analysis, it was further illustrated that miR181a expression and IL-15 production were enhanced during muscle mobilization, with higher magnitude in soleus than that in gastrocnemius (Figure 4G and

4H). Notably, up-regulation of miR181a was confirmed by FISH assay (Figure 4I).

Influence of macrophage phenotype and T cell activation on muscular function

The activity of MuSK and AChR clustering at motor endplates is required for nerve-muscle synapse formation, maintenance, and synaptic transmission. In nerve-muscle preparations, it was revealed that expressions of Grb2, PLC γ , p85, Vav, and HER2 were substantially decreased in the presence of IL-15 or M1- but not M2-conditioned medium (Figure 5A and 5B). Furthermore, as determined by MTT assay, we observed that cell survival was decreased in the presence of IL-15 or M1- but not M2-conditioned medium (Figure 5C). Likewise, MuSK activity and AChR clustering were suppressed following above treatment (Figure 5D and 5E).

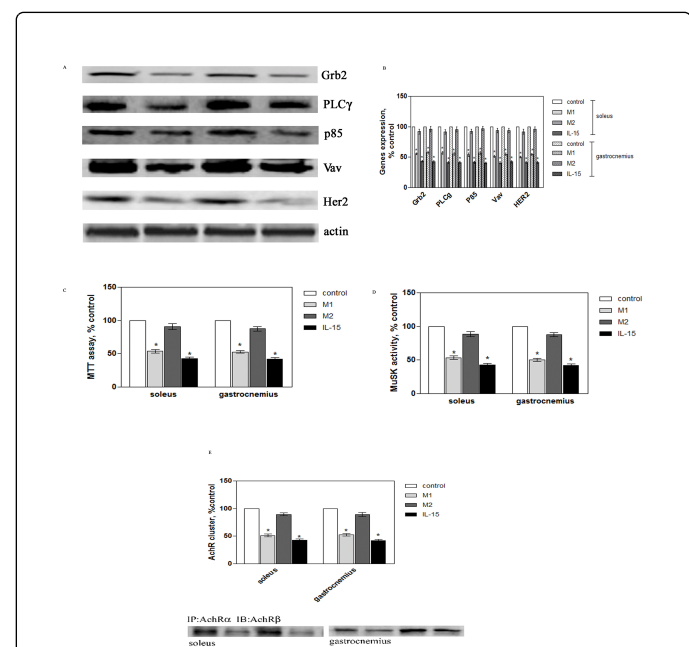


Figure 5: Influence of macrophage phenotype and T cell activation on muscular function. Nerve-muscles soleus and gastrocnemius were cultured in the presence of IL-15, M1 or M2 conditioned medium. A and B, expressions of receptor tyrosine kinase signaling molecules including Grb2, PLC γ , p85, Vav, HER2 were detected by Western Blot analysis; C, Muscle cell survival was determined by MTT assay; D, MuSK activity was detected by *in vitro* kinase assay; E, ACh cluster was measured by immunoprecipitation, in which anti-AchR α was used as an immunoprecipitated antibody and anti-achR β as an immunoblot antibody. Data are normalized and calculated as the percentage of control, each value is the mean ± S.E.M. for 5 independent experiments. *p<0.05 vs control.

VEGFR2 mitochondrial translocation is associated with motor endplate stability

Finally, it was demonstrated that cell viability was gradually reduced following muscle mobilization, the effect could be deteriorated upon mitoVEGFR2 infection, intriguingly, the reduction was more apparent

in soleus than in gastrocnemius muscle (Figure 6A). Similarly alteration was observed in MuSK activity and AChR clustering (Figure 6B-6D). In addition, mechanical power was greatly diminished following 7 days of muscle mobilization, which could be further inhibited when infection of mitoVEGFR2. Also, the inhibition displayed exhibited with higher magnitude in soleus than in gastrocnemius muscle (Figure 6E).

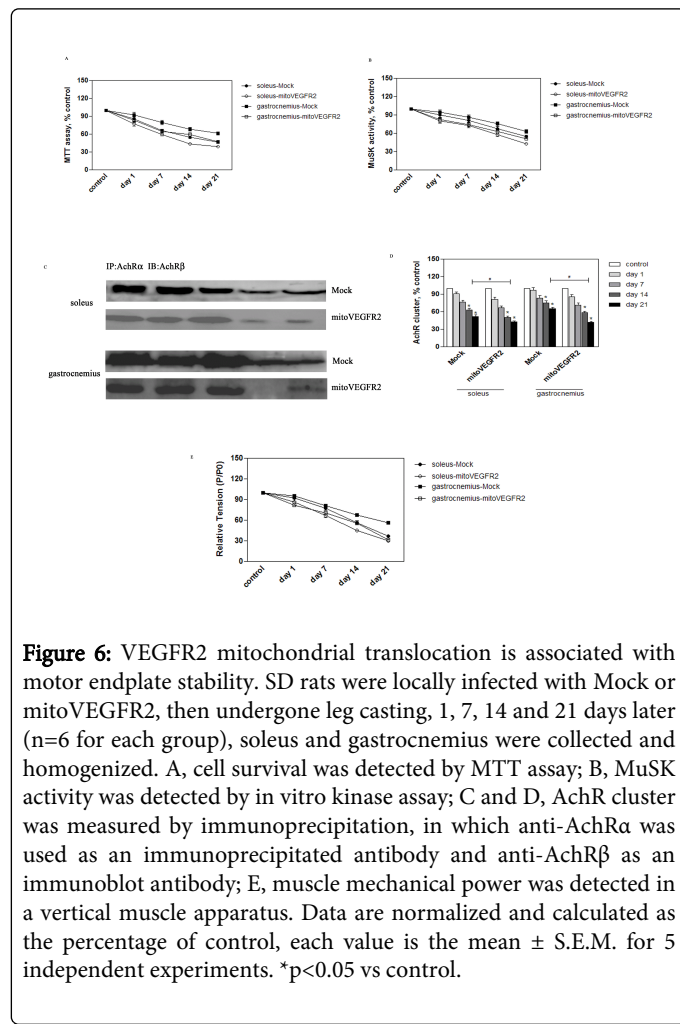


Figure 6: VEGFR2 mitochondrial translocation is associated with motor endplate stability. SD rats were locally infected with Mock or mitoVEGFR2, then undergone leg casting, 1, 7, 14 and 21 days later ($n=6$ for each group), soleus and gastrocnemius were collected and homogenized. A, cell survival was detected by MTT assay; B, MuSK activity was detected by in vitro kinase assay; C and D, AchR cluster was measured by immunoprecipitation, in which anti-AchR α was used as an immunoprecipitated antibody and anti-AchR β as an immunoblot antibody; E, muscle mechanical power was detected in a vertical muscle apparatus. Data are normalized and calculated as the percentage of control, each value is the mean \pm S.E.M. for 5 independent experiments. * $p<0.05$ vs control.

Discussion

We previously reported that timely activation of receptor tyrosine kinases was responsible for early muscular inflammation in the denervated gastrocnemius, and that a balance between VEGFR1 and VEGFR2 in the plasma membrane dictated negative or positive responses to muscle function [12]. In the present study, VEGFR2 was found to be specifically recruited by MyHCl and MyHC2B in gastrocnemius and soleus muscles respectively, the distinctive connection was presumed to be associated with activation of downstream molecules including Grb2, PLC γ , p85, Vav, and HER2. Since VEGFR2 was reported to protect gastrocnemius muscle from denervation-induced atrophy via vascular remodeling, tissue growth and differentiation [32-35]. In addition, accumulating evidence indicated that the degree of muscle denervation depends on muscle type, with atrophy more prominent in type I than in type II muscle fibers. Then, it was hypothesized that the recruitment of VEGFR2 to

MyHC might restrict distinctive regulatory components in fast and slow muscles during muscle injury.

Lately, it was reported that there is a differential turnover of myosin heavy chain (MyHC) proteins during muscle wasting [25-29]. Then, mobilization of gastrocnemius and soleus was established in the present study, wherein distinctive VEGFR2 trafficking was evoked. In gastrocnemius, we demonstrated that VEGFR2 signaling was translocated into mitochondria at later stages of mobilization, which accompanied with mitochondrial alteration including increased DNA content and induction of NAD $^+$ -SirT1 signaling. As well known, denervation causes a rapid alteration in mitochondrial function in muscle fibers, thereby promoting protein breakdown and muscle fiber atrophy [36,37]. Thereby, the specific responses in gastrocnemius to mobilization may be explained by VEGFR2 mitochondrial transportation. Moreover, it was illustrated that M1 and M2 macrophages was rapidly polarized in the mobilized gastrocnemius, and M2 macrophage polarization required a highly activation of VEGFR2 mitochondrial translocation and NAD $^+$ -SirT1 signaling, together with other report on a molecular link between metabolism and the epigenetic regulation of proinflammatory genes [6-9], as such, the present observation indicated that VEGFR2 mitochondrial translocation was mostly implicated in gastrocnemius mobilization, by which triggered a dramatic increase in NAD phosphate oxidase activity and dampened M2 polarization.

Alternatively, in the mobilized soleus, VEGFR2 was transported to ER, this short-range transport resulted in T cell activation, evidenced by calreticulin membrane expression, miR181a up-regulation and IL-15 production, then, in one hand, the observation was in agreement with previous report that VEGFR trafficking was related with functional alteration in ER and Golgi complex [38-42], in other hand, it was proposed that mobilized soleus provided distinct microenvironments from gastrocnemius. In addition, it was demonstrated that M1 but not M2 macrophage was predominantly polarized in soleus during muscle mobilization. Therefore, it was presumed that on account of absent VEGFR2 initiated mitochondrial responses, M1 macrophage polarization and T cell activation made soleus more vulnerable to insults than gastrocnemius. As expected, it was demonstrated that muscle function including receptor tyrosine kinase activation, cell survival, and end-plate stability [43-45] was deteriorated as a result of M1 macrophage polarization or IL-15 exposure, but was mostly stable in the presence of the M2 phenotype. Thereby, we assumed that there was a regulatory loop that modulated the muscular function, during muscle mobilization, early preferential M2 macrophage polarization might prolong gastrocnemius activity, while vulnerability to T cell activation was typically associated with soleus damage.

Finally, we showed that VEGFR2 mitochondrial targeting during muscle mobilization was accompanied by a decline in functional motor endplates and muscle mechanical power, and with rapid ratio than that of vehicle injection, intriguingly, the degradation could be observed similarly in soleus and gastrocnemius. Thus, the compartmentalization of VEGFR2 by myosin is likely a key mechanism in the maintenance of muscle function, muscle mobilization initiated differential VEGFR2 trafficking in gastrocnemius and soleus, the evolved macrophage polarization and T cell activation were contributed to respective muscle activity.

Altogether, the results of the present study demonstrated association between VEGFR2 and MyHCl in gastrocnemius, VEGFR2 and MyHC2B in soleus, which was likely responsible for the activation

of downstream molecules including Grb2, PLC γ , p85, Vav, and HER2. Upon muscle mobilization, translocation of VEGFR2 into mitochondria was ultimately initiated in gastrocnemius, which resulted in reinforced NAD $^{+}$ -SIRT1 signaling and dampened M2 macrophage responses. Comparably, in soleus muscle, VEGFR2 was targeted to ER compartment, this short-range transport eventually enhanced subsequent T cell activation. Importantly, M1 macrophage polarization and T cell activation mostly induced disrupted muscular homeostasis, the cellular processes might make soleus more vulnerable to insults than gastrocnemius. Therefore, it is likely that distinctive endocytic delivery of VEGFR2 cargo might facilitate certain microenvironment in the mobilized gastrocnemius and soleus, and led to respective muscle damage. A better understanding of phenotype-dependent alterations in muscle would enable the development of new agents to combat degenerative muscular disorders.

Acknowledgment

This work is supported by the Natural scientific program in Minhang District of Shanghai (2011MHZ21), National nature sciences of China (81471370).

References

1. Apidianakis Y, Mindrinos MN, Xiao W, Tegos GP, Papisov MI, et al. (2007) Involvement of skeletal muscle gene regulatory network in susceptibility to wound infection following trauma. *PLoS One* 2: e1356.
2. Marino M, Scuderi F, Provenzano C, Bartoccioni E (2011) Skeletal muscle cells: from local inflammatory response to active immunity. *Gene Ther* 18: 109-116.
3. Conley KE, Jubrias SA, Esselman PC (2000) Oxidative capacity and ageing in human muscle. *J Physiol* 526 Pt 1: 203-210.
4. Wicks KL, Hood DA (1991) Mitochondrial adaptations in denervated muscle: relationship to muscle performance. *Am J Physiol* 260: C841-850.
5. Siu PM, Alway SE (2005) Mitochondria-associated apoptotic signalling in denervated rat skeletal muscle. *J Physiol* 565: 309-323.
6. Araki T, Sasaki Y, Milbrandt J (2004) Increased nuclear NAD biosynthesis and SIRT1 activation prevent axonal degeneration. *Science* 305: 1010-1013.
7. Brunet A, Sweeney LB, Sturgill JF, Chua KF, Greer PL, et al. (2004) Stress-dependent regulation of FOXO transcription factors by the SIRT1 deacetylase. *Science* 303: 2011-2015.
8. Daitoku H, Hatta M, Matsuzaki H, Aratani S, Ohshima T, et al. (2004) Silent information regulator 2 potentiates Foxo1-mediated transcription through its deacetylase activity. *Proc Natl Acad Sci U S A* 101: 10042-10047.
9. Tonkin J, Villarroya F, Puri PL, Vinciguerra M (2012) SIRT1 signaling as potential modulator of skeletal muscle diseases. *Curr Opin Pharmacol* 12: 372-376.
10. Jones WS, Duscha BD, Robbins JL, Duggan NN, Regensteiner JG, et al. (2012) Alteration in angiogenic and anti-angiogenic forms of vascular endothelial growth factor-A in skeletal muscle of patients with intermittent claudication following exercise training. *Vasc Med* 17: 94-100.
11. Tang K, Breen EC, Gerber HP, Ferrara NM, Wagner PD (2004) Capillary regression in vascular endothelial growth factor-deficient skeletal muscle. *Physiological Genomics* 18: 63-69.
12. Zhao H, Huang HW, Wu JG, Huang PY (2013) Specialization of mitochondrial and vascular oxidant modulated VEGFR in the denervated skeletal muscle. *Cell Signal* 25: 2106-2114.
13. Arnold L, Henry A, Poron F, Baba-Amer Y, van Rooijen N, et al. (2007) Inflammatory monocytes recruited after skeletal muscle injury switch into antiinflammatory macrophages to support myogenesis. *J Exp Med* 204: 1057-1069.
14. Kharraz Y, Guerra J, Mann CJ, Serrano AL, Muñoz-Cánoves P (2013) Macrophage plasticity and the role of inflammation in skeletal muscle repair. *Mediators Inflamm* 2013: 491497.
15. Segawa M, Fukada S, Yamamoto Y, Yahagi H, Kanematsu M, et al. (2008) Suppression of macrophage functions impairs skeletal muscle regeneration with severe fibrosis. *Exp Cell Res* 314: 3232-3244.
16. Smith C, Kruger MJ, Smith RM, Myburgh KH (2008) The inflammatory response to skeletal muscle injury: illuminating complexities. *Sports Med* 38: 947-969.
17. Tidball JG, Berchenko E, Frenette J (1999) Macrophage invasion does not contribute to muscle membrane injury during inflammation. *J Leukoc Biol* 65: 492-498.
18. Tidball JG, Wehling-Henricks M (2007) Macrophages promote muscle membrane repair and muscle fibre growth and regeneration during modified muscle loading in mice *in vivo*. *J Physiol* 578: 327-336.
19. Mantovani A, Sica A, Sozzani S, Allavena P, Vecchi A, et al. (2004) The chemokine system in diverse forms of macrophage activation and polarization. *Trends Immunol* 25: 677-686.
20. Gordon S (2003) Do macrophage innate immune receptors enhance atherogenesis? *Dev Cell* 5: 666-668.
21. Gordon S, Martinez FO (2010) Alternative activation of macrophages: mechanism and functions. *Immunity* 32: 593-604.
22. Gordon S, Taylor PR (2005) Monocyte and macrophage heterogeneity. *Nat Rev Immunol* 5: 953-964.
23. Olefsky JM, Glass CK (2010) Macrophages, inflammation, and insulin resistance. *Annu Rev Physiol* 72: 219-246.
24. Schiaffino S, Reggiani C (2011) Fiber types in mammalian skeletal muscles. *Physiol Rev* 91: 1447-1531.
25. Reid B, Martinov VN, Njå A, Lømo T, Bewick GS (2003) Activity-dependent plasticity of transmitter release from nerve terminals in rat fast and slow muscles. *J Neurosci* 23: 9340-9348.
26. Marshall JM, Tandon HC (1984) Direct observations of muscle arterioles and venules following contraction of skeletal muscle fibres in the rat. *J Physiol* 350: 447-459.
27. Fitts RH, Romatowski JG, Blaser C, De La Cruz L, Gettelman GJ, et al. (2000) Effect of spaceflight on the isotonic contractile properties of single skeletal muscle fibers in the rhesus monkey. *J Gravit Physiol* 7: S53-54.
28. Widrick JJ, Romatowski JG, Norenberg KM, Knuth ST, Bain JL, et al. (2001) Functional properties of slow and fast gastrocnemius muscle fibers after a 17-day spaceflight. *J Appl Physiol* (1985) 90: 2203-2211.
29. Stelzer JE, Widrick JJ (2003) Effect of hindlimb suspension on the functional properties of slow and fast soleus fibers from three strains of mice. *J Appl Physiol* (1985) 95: 2425-2433.
30. Andersen JL, Gruschy-Knudsen T, Sandri C, Larsson L, Schiaffino S (1999) Bed rest increases the amount of mismatched fibers in human skeletal muscle. *J Appl Physiol* (1985) 86: 455-460.
31. Tiwari A, Jung JJ, Inamdar SM, Nihalani D, Choudhury A (2013) The myosin motor Myo1c is required for VEGFR2 delivery to the cell surface and for angiogenic signaling. *Am J Physiol Heart Circ Physiol* 304: H687-696.
32. Ciurea R, Margaritescu C, Simionescu C, Stepan A, Ciurea M (2011) VEGF and his R1 and R2 receptors expression in mast cells of oral squamous cells carcinomas and their involvement in tumoral angiogenesis. *Romanian J Morphol Embryol* 52: 1227-1232.
33. Hirashima M, Ogawa M, Nishikawa S, Matsumura K, Kawasaki K, et al. (2003) A chemically defined culture of VEGFR2+ cells derived from embryonic stem cells reveals the role of VEGFR1 in tuning the threshold for VEGF in developing endothelial cells. *Blood* 101: 2261-2267.
34. Mittar S, Ulyatt C, Howell GJ, Bruns AF, Zachary I, et al. (2009) VEGFR1 receptor tyrosine kinase localization to the Golgi apparatus is calcium-dependent. *Exp Cell Res* 315: 877-889.

35. Zhang Z, Neiva KG, Lingen MW, Ellis LM, Nör JE (2010) VEGF-dependent tumor angiogenesis requires inverse and reciprocal regulation of VEGFR1 and VEGFR2. *Cell Death Differ* 17: 499-512.
36. Brault V, Reedy MC, Sauder U, Kammerer RA, Aebi U, et al. (1999) Substitution of flight muscle-specific actin by human (beta)-cytoplasmic actin in the indirect flight muscle of *Drosophila*. *J Cell Sci* 112 : 3627-3639.
37. Cohen S, Brault JJ, Gygi SP, Glass DJ, Valenzuela DM, et al. (2009) During muscle atrophy, thick, but not thin, filament components are degraded by MuRF1-dependent ubiquitylation. *J Cell Biol* 185: 1083-1095.
38. Barylko B, Jung G, Albanesi JP (2005) Structure, function, and regulation of myosin 1C. *Acta Biochim Pol* 52: 373-380.
39. Holt JR, Gillespie SK, Provance DW, Shah K, Shokat KM, et al. (2002) A chemical-genetic strategy implicates myosin-1c in adaptation by hair cells. *Cell* 108: 371-381.
40. McConnell RE, Tyska MJ (2010) Leveraging the membrane - cytoskeleton interface with myosin-1. *Trends Cell Biol* 20: 418-426.
41. Montes de Oca G, Lezama RA, Mondragón R, Castillo AM, Meza I (1997) Myosin I interactions with actin filaments and trans-Golgi-derived vesicles in MDCK cell monolayers. *Arch Med Res* 28: 321-328.
42. Neuhaus EM, Soldati T (2000) A myosin I is involved in membrane recycling from early endosomes. *J Cell Biol* 150: 1013-1026.
43. Punga AR, Maj M, Lin S, Meinen S, Rüegg MA (2011) MuSK levels differ between adult skeletal muscles and influence postsynaptic plasticity. *Eur J Neurosci* 33: 890-898.
44. Rivas-Plata KA, Kraas JR, Saleh SM, Swope SL (2001) Src-class kinases act within the agrin/MuSK pathway to regulate acetylcholine receptor phosphorylation, cytoskeletal anchoring, and clustering. *J Neurosci* 21: 3806-3818.
45. Smith CL, Mittaud P, Prescott ED, Fuhrer C, Burden SJ (2001) Src, Fyn, and Yes are not required for neuromuscular synapse formation but are necessary for stabilization of agrin-induced clusters of acetylcholine receptors. *J Neurosci* 21: 3151-3160.